# Isostructural phase transition of $Fe_2O_3$ under laser shock compression

A. Amouretti,[1,2,*] C. Crépisson,[3,†] S. Azadi,[3] F. Brisset,[4] D. Cabaret,[1] T. Campbell,[3] D. A. Chin,[5] G. W. Collins,[5] L. Hansen,[5] G. Fiquet,[1] A. Forte,[3] T. Gawne,[3] F. Guyot,[1] P. Heighway,[3] E. Heriprë,[6] E. Cunningham,[7] H. J. Lee,[7] D. McGonegle,[8] B. Nagler,[7] J. Pintor,[1] D. N. Polsin,[5] G. Rousse,[9,10] Y. Shi,[3] E. Smith,[5] J. S. Wark,[3] S. M. Vinko,[3,11] and M. Harmand[1,6]

[1] *IMPMC, Sorbonne Université, UMR CNRS 7590, MNHN, 75005 Paris, France*
[2] *Graduate School of Engineering, Osaka University, Suita, Osaka 565-0871, Japan*
[3] *Department of Physics, Clarendon Laboratory, University of Oxford, Parks Road, Oxford OX1 3PU, UK*
[4] *Université Paris-Saclay, CNRS, Institut de chimie moléculaire et des matériaux d'Orsay, Orsay 91405, France*
[5] *University of Rochester Laboratory for Laser Energetics, Rochester, NY, USA*
[6] *PIMM, Arts et Metiers Institute of Technology, CNRS, CNAM, HESAM University, 151 boulevard de l'Hopital, 75013 Paris, France*
[7] *SLAC National Accelerator Laboratory, 2575 Sand Hill Rd, Menlo Park, CA 94025, USA*
[8] *AWE, Aldermaston, Reading, RG7 4PR, United Kingdom*
[9] *CSE Lab, UMR 8260, Collège de France, 75231 Paris Cedex 05, France*
[10] *Sorbonne Université, 4 place Jussieu, 75005 Paris, France*
[11] *Central Laser Facility, STFC Rutherford Appleton Laboratory, Didcot OX11 0QX, UK*

(Dated: March 22, 2025)

We present *in-situ* x-ray diffraction and velocity measurements of $Fe_2O_3$ under laser shock compression at pressures between 38-122 GPa. None of the high-pressure phases reported by static compression studies were observed. Instead, we observed an isostructural phase transition from $\alpha$-$Fe_2O_3$ to a new $\alpha'$-$Fe_2O_3$ phase at a pressure of 50-62 GPa. The $\alpha'$-$Fe_2O_3$ phase differs from $\alpha$-$Fe_2O_3$ by an 11% volume drop and a different unit cell compressibility. We further observed a two-wave structure in the velocity profile, which can be related to an intermediate regime where both $\alpha$ and $\alpha'$ phases coexist. Density functional theory calculations with a Hubbard parameter indicate that the observed unit cell volume drop can be associated with a spin transition following a magnetic collapse.

The phase diagrams of iron oxides are notoriously rich with a variety of electronic and structural transitions triggered by pressure or temperature. Due to its relevance to geophysical studies, $Fe_2O_3$ has been extensively studied under static compression using Laser Heated Diamond Anvil Cells (LH-DAC), up to approximately 113 GPa and 2800 K [1–3]. A series of phase transitions were observed, as well as a possible breakdown of $Fe_2O_3$ at high temperature into $Fe_{25}O_{32}$ and $Fe_5O_7$ [1]. Moreover, a Mott transition and a high-spin to low-spin transition have been evidenced at ∼50 GPa, although it remains unclear if structural transitions are triggered by the electronic transition or vice versa [4–7]. The $\alpha$-$Fe_2O_3$ phase ($R\bar{3}c$) is stable up to 40 GPa. For this phase, a continuous decrease in the c/a ratio is observed with increasing pressure [8–12]. From 40 GPa to 47 GPa, the $\iota$-$Fe_2O_3$ phase ($Rh_2O_3$-II type structure, *Pbcn* orthorhombic) is observed [1, 13]. Above ∼54 GPa, the $\iota$ phase transforms into $\zeta$-$Fe_2O_3$ phase (a distorted perovskite described in the monoclinic system [8]) stable up to 55 GPa. Above 50-60 GPa, the $\zeta$-$Fe_2O_3$ phase transforms into $\eta$-$Fe_2O_3$ (*Cmcm* post-perovskite orthorhombic), while above 67 GPa the possibly metastable $\theta$-$Fe_2O_3$ (*Aea*2 orthorhombic), is also observed in a limited region between approximately 1000 and 2000 K [1].

Laser-based dynamic compression enables extending *in situ* phase diagram studies to higher pressures than reached by static compression. For that reason, it has been extensively used to infer mineral properties in planetary and exoplanetary interiors [14–16]. However, the timescales under which phase transformations take place in such experiments are on the order of tens of picoseconds up to microseconds in release, much shorter than the typical planetary timescale. It is thus important to understand the limitations of dynamic compression experiments, in particular when used to inform geophysical studies. Unfortunately, the behaviour of dynamically compressed $Fe_2O_3$ is poorly understood and experimental results are scarce, largely due to the complexity of target design [17, 18]. Nevertheless, gas gun measurements performed up to 140 GPa [17, 19] show a significant volume drop of ∼10% at approximately 50 GPa, which may be indicative of the transitions observed statically. Another study reported a significant drop in resistivity at ∼44-52 GPa using a double-stage light-gas gun on large natural $Fe_2O_3$ crystals, which can be linked to the Mott transition [18]. However, the crystal structures of $Fe_2O_3$ under shock compression are unknown, and it remains unclear how these relate to the flurry of phases observed under static compression.

In this letter we present *in-situ* time-resolved x-ray diffraction measurements in shock-compressed $Fe_2O_3$ using an x-ray Free Electron Laser (XFEL), at pressures between 38-122 GPa. Our results demonstrate that the behaviour of $Fe_2O_3$ is indeed very different under dynamic compression: we observe none of the high-pressure phases

seen statically, and instead find a single new isostructural phase transition at 50-62 GPa, which we link to a collapse in magnetic ordering.

The experiment was performed at the Matter in Extreme Condition (MEC) end station of the Linac Coherent Light Source (LCLS) [20]. The shock was driven by two synchronized nanosecond lasers (527 nm) incident on the target at an angle of 20° and with a spot size of 300 $\mu$m. We used pulse durations of 5, 10 and 15 ns, with a maximum total energy of 60 J on target. *In-situ* x-ray diffraction (XRD) was performed using the x-ray beam operating in self-amplified spontaneous emission mode, with a photon energy of 7.08 keV, a spectral bandwidth of 25 eV, and pulse duration of 50 fs FWHM [21, 22]. The x-rays were focused onto the target at an angle of 35° with a spot size diameter of 60 $\mu$m, overlapping the focal spot of the optical lasers to probe the planar shock front region. The diffraction signal was measured in transmission geometry on 4 quadruple ePix10k detectors. Azimuthal integration of 2D diffraction images was carried out including solid angle correction, Al filter correction, polarization, and self-attenuation from the target. When this was not possible, integration was performed using the Dioptas software, based on the PyFai library [23, 24], including solid angle correction and polarization. Two Velocity Interferometer System for Any Reflector (VISAR) [25] were used to retrieve the particle velocity and the time when the shock left the $Fe_2O_3$ sample, and determine the Hugoniot pressure for each data point. VISAR sensitivities were 4.5241 and 1.9890 km $s^{-1}$ $fringes^{-1}$, respectively, with related acquisition time windows of 10 and 20 ns. Two target designs (detailed in SI Section A [26]) were used during the experiment: (1) a 8 $\mu$m $Fe_2O_3$ layer sandwiched between a sapphire window and a parylene-N ablator allowing direct measurement of the particle velocity and (2) a 8 $\mu$m $Fe_2O_3$ layer on a parylene-N ablator aiming to optimize the XRD signal. $Fe_2O_3$ was deposited by Physical Vapor Deposition (PVD) and shows a polycrystalline structure of columnar crystallites with preferential orientation (SI section B, C, D [26]).

We show the radially integrated x-ray diffraction patterns of $Fe_2O_3$ under shock in Fig. 1, measured when nearly the entire $Fe_2O_3$ layer is shocked, but before shock breakout and release. The pattern recorded prior to the shock at ambient conditions is shown for comparison. At pressures below 42 GPa, the patterns (i) and (ii) show similar features to that of the ambient sample in terms of both peak positions and intensities. Nine $\alpha$-$Fe_2O_3$ peaks are identified and shifted toward larger angles due to sample compression. Overall, strong peak broadening is observed in shocked samples, reminiscent of a decrease in crystallite size and an increase in micro-strain effects (lattice parameters fluctuations) under pressure [28, 29]. At intermediate pressures, patterns (iii) and (iv) show four additional peaks, indexed in red on pattern (iii).

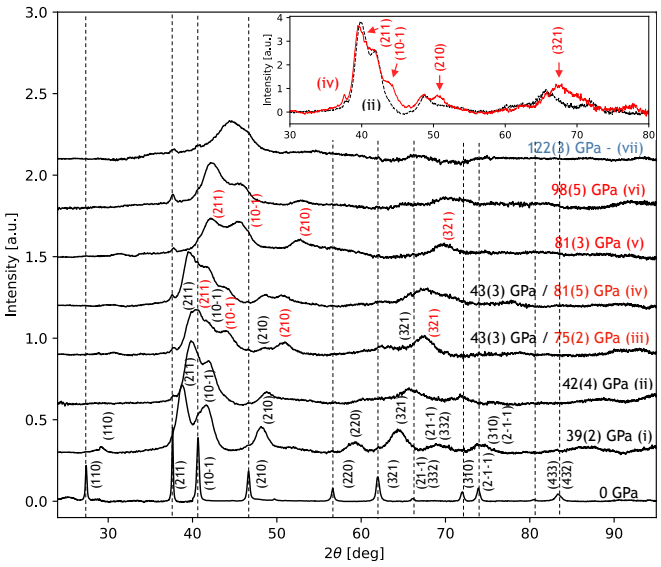


FIG. 1. Radially integrated x-ray diffraction profiles of $Fe_2O_3$ under shock for targets with a sapphire window between 0-122 GPa. The vertical dotted lines corresponds to the ambient $\alpha$-$Fe_2O_3$ peak positions [27]. Miller (hkl) indices are displayed for the low- and high-pressure $\alpha$ structures in black and red, respectively. The inset highlights differences between patterns (ii) and (iv). The two pressures indicated for pattern (iii) and (iv) correspond to the two phases observed in diffraction, and are determined based on VISAR analysis of the double wave structure observed for those data points (fig. 3).

We attribute these to the appearance of a second kind of $Fe_2O_3$ phase, which we dub the $\alpha'$ phase, having the same crystallographic structure as $\alpha$ but a significantly lower volume. These mixed patterns are thus associated with two pressures, depending on the phase. For pressures above 81 GPa, only four peaks corresponding to the $\alpha'$-$Fe_2O_3$ are observed, with a significant shift toward larger angles due to larger compression. At 122 GPa, pattern (vii) shows the disappearance of the diffraction peaks and the appearance of a diffuse signal at scattering angles of 45° ($Q = 2.7$ Å$^{-1}$) and 55° ($Q = 3.4$ Å$^{-1}$), which could be interpreted as an amorphous phase (2D diffraction data are shown in Fig. S12 [26]).

It was not possible to perform Rietveld refinements on the data due to the complex microstructure of the samples under shock. Instead, we performed Le Bail refinements, shown in Fig. 2, for data from targets without a sapphire window. At 47(1) GPa a decrease of $c/a$ ratio for the compressed $\alpha$-$Fe_2O_3$ phase is observed compared with ambient $\alpha$-$Fe_2O_3$. At 94(2) GPa we identify an $\alpha$-$Fe_2O_3$ structure with a significantly smaller volume than the $\alpha$-$Fe_2O_3$ observed at 47(1) GPa (225.2 Å$^3$ and 265.8 Å$^3$, respectively). In both cases, the $\alpha$-$Fe_2O_3$ structure [27] fits the compressed phase well ($R_p = 12.4\%$). The temperature is expected to vary from 400 K at 39 GPa, to 1400 K at 116 GPa, along the $Fe_2O_3$ Hugo-

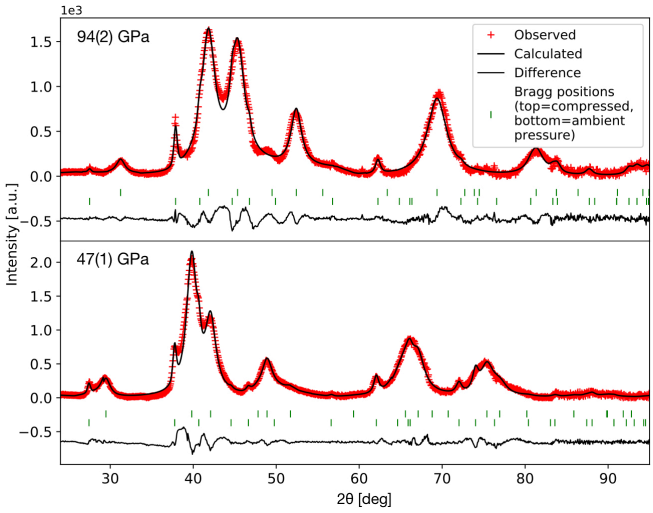


FIG. 2. Le Bail refinements of two radially integrated x-ray diffraction patterns for targets without sapphire window probed just before shock breakout, at pressures of 47(1) GPa and 94(2) GPa. Each pattern was fitted using two $\alpha$-$Fe_2O_3$ phases with $R\bar{3}c$ symmetry: one for the $\alpha$-$Fe_2O_3$ ambient at 0 GPa (bottom green tick marks) and one for the compressed $\alpha$-$Fe_2O_3$ phase (top green tick marks). $R_p$ factors were 10.5% and 12.4% for the 47 GPa and 94 GPa patterns, respectively. Fitted lattice parameters are $a_0 = 5.03$ Å; $c_0 = 13.03$ Å for ambient $\alpha$-$Fe_2O_3$; $a = 4.87(2)$ Å; $c = 12.94(2)$ Å for 47 GPa; and $a = 4.56(2)$ Å; $c = 12.54(2)$ Å for 94 GPa.

niot based on SESAME 7440 [30]. The $Fe_2O_3$ Hugoniot thus passes through all stability fields of $Fe_2O_3$ phases observed under static compression. However, none of the high-pressure phases of $Fe_2O_3$ reported under static compression were observed ($\iota$-$Fe_2O_3$, $\zeta$-$Fe_2O_3$, $\eta$-$Fe_2O_3$, $\theta$-$Fe_2O_3$, $Fe_{25}O_{32}$, or $Fe_5O_7$ [1]).

Velocity profiles at the $Fe_2O_3$/Sapphire interface for increasing laser intensities are shown as a function of time in Fig. 3. A double-wave structure is systematically observed in VISAR data when the mixing of the $\alpha$ and $\alpha'$ phases is detected in diffraction, as shown for shots in blue. The first wave is labelled P1 and the second wave P2. From the appearance of the $\alpha'$ phase, the P1 wave velocity remains constant at around 1.3 km $s^{-1}$ for all mixed shots regardless of the laser intensity. In contrast, the P2 wave velocity increases with laser intensity and its arrival time becomes shorter. The double-wave structure is also observed for targets without a sapphire window, measured directly from the free surface of $Fe_2O_3$ (Fig. S11 [26]). This indicates that the double-wave structure is not due to the sapphire window, but is produced within the $Fe_2O_3$ layer at specific laser intensities. The splitting of the wavefront into two waves is characteristic of a phase transition with a volume change [31, 32]. We thus identify this observation as a signature of the $\alpha \rightarrow \alpha'$ phase transition, which is also observed in diffraction, and associate the P1 and P2 waves with the $\alpha$ and $\alpha'$ phases, respectively. The pressures in the $\alpha$ and $\alpha'$ phases can then be determined from the P1 and P2 velocities, similarly to previous work on Bismuth [33].

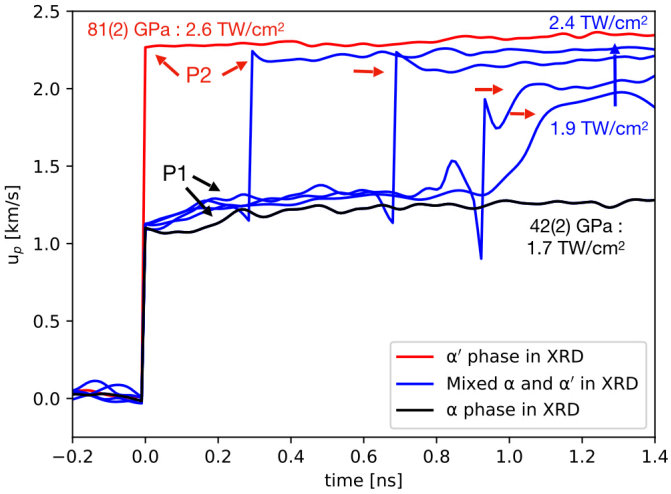


FIG. 3. Particle velocities measured at the rear of the $Fe_2O_3$ sample for the different pressure regimes. The time origin is set to the shock breakout time in the sapphire. In black we show a low-pressure shock where only a single $\alpha$ phase is observed in x-ray diffraction. The blue curves, taken at intensities between 1.9 and 2.4 TW/$cm^2$, correspond to thermodynamic conditions where both $\alpha$ and $\alpha'$ are observed in diffraction. The red curve corresponds to conditions where only a single compressed $\alpha'$ phase is observed. The double-wave structure is indicative of a phase transition.

The unit cell volumes of the $\alpha$-$Fe_2O_3$ and $\alpha'$-$Fe_2O_3$ phases are plotted against pressure in Fig 4. The $\alpha$-$Fe_2O_3$ phase is observed up to 54 ± 2 GPa, and the $\alpha'$-$Fe_2O_3$ phase for pressures above 63 ± 2 GPa. We measure a (11.0 ± 1.4)% volume drop between the two phases, calculated from x-ray diffraction data showing both in coexistence. This volume drop indicates that the transition from $\alpha$ to $\alpha'$ is a first-order transition.

We acknowledge a pressure gap of 9 ± 3 GPa in our dataset. This could be due to experimental detection limitations, such as 1) the VISAR etalon; 2) the temporal range restricted by the multiple waves in our sample design (see Fig. S6 of the supplementary [26]) that might prevent the detection of the P2 waves with breakout time superior to the temporal range; or 3) the inherent laser-shocked x-ray diffraction peak width, which prevents small $\alpha'$ peaks to be observed. In addition, phase transitions under shock are also subject to temperature effects that might broaden the transition pressure range [31], as well as superheating, kinetic and plasticity effects [34–36] that might affect the onset pressure for $\alpha'$-$Fe_2O_3$ synthesis.

Overall, our data yield larger unit cell volumes than previous shock data from gas gun experiments [19] as seen in Fig. 4. However, these previous measurements are intrinsically different to ours, either due to the com-

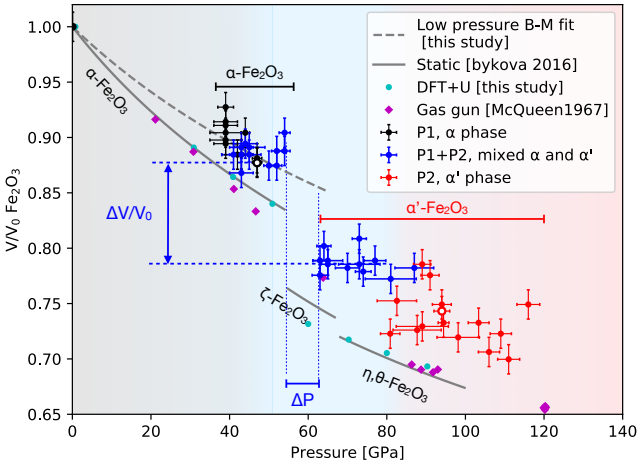


FIG. 4. $V/V_0$ for $\alpha$-$Fe_2O_3$ and $\alpha'$-$Fe_2O_3$ determined from x-ray diffraction as a function of pressure, compared with other published work. Points corresponding to the observation of only the $\alpha$-$Fe_2O_3$ phase are plotted in black, of only the $\alpha'$-$Fe_2O_3$ phase in red, and of the coexistence of both phases in blue. The two empty symbols correspond to data points determined from the Le Bail fits shown in Fig. 2. A transition from $\alpha$-$Fe_2O_3$ to $\alpha'$-$Fe_2O_3$ phase is observed at 54-62 GPa. It is associated with a relative volume jump $\Delta V/V_0$ equal to 11.0 % and pressure jump of $\Delta P \sim 9$ GPa. A second-order Birch-Murnaghan fit (B-M fit represented with grey dotted line) has been performed for the $\alpha$ phase (see section K of the SI [26]). The relative volume jump between the extrapolated volume for the $\alpha$ phase at 63-65 GPa and the measured volume for the $\alpha'$ phase at the same pressure is 7.7%.

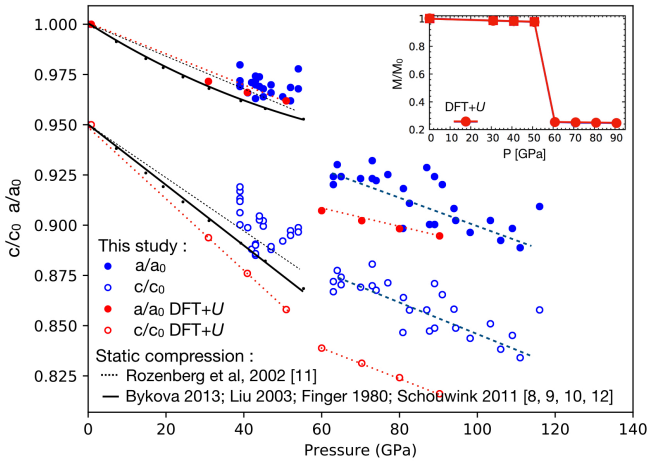


FIG. 5. Lattice parameters for the $\alpha$ and $\alpha'$ phases as a function of pressure. All $c/c_0$ data are shifted vertically by -0.05 for clarity. Shock data are represented by solid blue dots ($a/a_0$) and empty blue dots ($c/c_0$). Dashed blue lines above 60 GPa are drawn to guide the eye. The c/a ratio is shown to vary with pressure for the $\alpha$ phase while it remains constant at 2.73 for the $\alpha'$ phase. Lattice parameters for the $\alpha$ phase from static compression are given as solid black lines for ref. [8–10, 12] and black dotted line for ref. [11]. The results from DFT+$U$ using a rhombohedral phase are given in red. The inset figure shows the relative magnetic moment of Fe from DFT+$U$ as a function of pressure. The phase is high spin below 50 GPa, and low spin above 60 GPa.

pression strain rate (from $10^5$ for gas gun measurement to $10^9$ for laser-driven shock compression [37]), the time during which the sample remains under pressure (several hundreds of ns for previous gas gun measurement on $Fe_2O_3$ [18, 19]), or by the nature of the measurements (optical and macroscopic compared with x-ray bulk and microscopic). In this work, the volume is extracted from the positions of the diffraction peaks. Further, we note that $Fe_2O_3$ single-crystals are known to behave differently depending of the relative alignment of the compression direction with the crystal axis [18]. Because of how our samples were deposited they do have a notable preferred orientation, and this may well affect the experimental compression values.

Figure 5 shows the evolution of $a/a_0$ and $c/c_0$ ratios, where $a$ and $c$ denote the lattice parameters under shock and $a_0$ and $c_0$ the parameters at ambient conditions. Both are deduced from Le Bail refinements. Below 54 GPa, the ratios for $\alpha$-$Fe_2O_3$ are consistent with static compression data [11], and can be explained by bonding distortion or uneven modifications of the Fe-O-Fe bond lengths [8–12]. This pressure distortion effect is observed in other corundum-structured oxides [8, 38], and can lead to a Mott insulator transition. A discontinuity of 3.6 % is seen between 54-62 GPa for $a/a_0$, in line with the observed volume drop between the $\alpha$ and $\alpha'$ phases shown in Fig. 4. No discontinuity is observed for $c/c_0$. Above 62 GPa we observe a change in the slope of $c/c_0$ with pressure, while the slope of the corresponding $a/a_0$ line remains unchanged. This indicates that the $c$-axis becomes less compressible in the new $\alpha'$ phase, and that the volume drop observed is mostly due to a strong decrease of the $a$ lattice parameter.

As the transition is observed without change of symmetry, the $\alpha$-$Fe_2O_3$ to $\alpha'$-$Fe_2O_3$ transition could be electronically driven. Two electronic transitions are observed at 50 GPa in static compression experiments: a Mott transition and a simultaneous spin transition [7]. These transitions are not limited by the timescale required for atomic displacement, and can therefore be much faster than a structural transition. Moreover, it has been shown that Mott and spin transitions can lead to a significant volume collapse without structural change [7], as seen, for example, in MnO [39] and FeO [40]. To further investigate such electronic transitions, we performed DFT+$U$ calculations [41–46] of $\alpha$-$Fe_2O_3$ (see SI section L [26] for more detail).

The results of the DFT+$U$ calculations are shown in Figs. 4 and 5. All main features of interest observed experimentally around the phase transition at 50-60 GPa are reproduced in the simulations: we find a large $V/V_0$ volume drop (∼10%), a discontinuity in the evolution

of $a/a_0$ but without a change in compressibility, and a change in compressibility but without a discontinuity in $c/c_0$. While there remains some discrepancy in the absolute values for the calculated parameters, overall the simulations reproduce the observed trends with good fidelity. The volume drop between 50-60 GPa is correlated to a drop in the local magnetic momentum of iron, as shown in the inset in Fig. 5, decreasing by a factor of 5, i.e. changing from a high to a low spin state. Therefore, we posit that the $\alpha \rightarrow \alpha'$ transition could be explained by a spin transition from a high-spin rhombohedral phase ($\alpha$-$Fe_2O_3$) to a low-spin rhombohedral phase ($\alpha'$-$Fe_2O_3$ being a low-spin corundum-structured phase). While our DFT+$U$ calculations are not tailored to identify a Mott transition, it is known from dynamical mean-field theory calculations that the spin transition and the Mott transition are linked and occur simultaneously [47]. $Fe_2O_3$ undergoes an electronic phase transition independently of the pressure/temperature pathway, being associated with structural phase transition under static compression, but being isostructural upon static decompression [7] and under laser-shock compression. Furthermore, all the Fe atoms are in an octahedral site, favorable to high-spin to low-spin transition upon pressure increase [1, 7]. We thus propose that the $\alpha \rightarrow \alpha'$ transition here observed under laser shock compression is an electronically driven spin transition from high-spin to low-spin, possibly associated with a Mott transition. Importantly, this implies that the electronic transition occurs before any structural transition under shock compression. Previous static compression experiments reported simultaneous electronic (spin and Mott transitions) and structural transitions (to $\eta$ or $\theta$-$Fe_2O_3$ phases) [1–7].

To summarize, we have presented *in-situ* time-resolved x-ray diffraction measurements in shock-compressed $Fe_2O_3$ up to 122 GPa, showing a clear difference in the phase diagram compared with static compression experiments. None of the high pressure phases seen statically were observed dynamically. Instead, we observed an isostructural $\alpha \rightarrow \alpha'$ phase transition around 50-60 GPa, characterized by an 11% volume drop due to a high-spin to low-spin transition, and, possibly, a Mott transition. Our results thus show that the electronic transition(s) observed in $Fe_2O_3$ under static compression around 50 GPa still occur, but without the associated structural transitions. The effect of the microstructure of our initial sample, uniaxial compression and different pressure-temperature pathways and strain rates involved in static and dynamic compressions [37, 48] should be further explored. This structural phase transition might also require timescales longer than those accessible in our experiment to occur. The structures of the $\theta$ and $\eta$ phases differ significantly from the structure of the $\alpha$ phase: they are composed of $FeO_6$ prisms and octahedra, whereas the $\alpha$ phase is only composed of $FeO_6$ octahedra [1]. Our results thus suggest that the fast electronic transitions (<1 ns) are the ones driving the comparatively slower reconstructive structural transitions to the $\theta$ and $\eta$ phases (>1 ns) [49], and not vice versa. Although a variety of high-spin/low-spin volume jumps have been reported in static compression ([50, 51] and references therein), and inferred from Hugoniot discontinuities under dynamic compression [52–54], here, this volume jump is observed in-situ together with crystallographic measurements. It is the first time that an electronic transition is reported under dynamic compression, without the associated structural transition observed under static compression. Differences have already been reported between static and dynamic phase diagrams such as pressure lowering [34, 55], absence of phase transition [56] or shock amorphization [57]. Our results raise questions on the electronic phase transition mechanisms and kinetics occurring under shock compression, and highlight the need for further investigation.

Use of the Linac Coherent Light Source (LCLS), SLAC National Accelerator Laboratory, is supported by the U.S. Department of Energy, Office of Science, Office of Basic Energy Sciences under Contract No. DE-AC02-76SF00515. The MEC instrument is supported also by the U.S. Department of Energy Office of Science, Fusion Energy Science under Contract No. DE-AC02-76SF00515, FWP 100106. This project has received funding from the European Research Council (ERC) under the European Union's Horizon 2020 research and innovation program (ERC PLANETDIVE grant agreement No 670787). Part of the writing of the article was performed by A. Amouretti as an JSPS International Research Fellow (Postdoctoral Fellowships for Research in Japan). C.C., S.A., P.H., J.S.W and S.M.V. acknowledge support from the UK EPSRC under grants EP/P015794/1, EP/W010097/1 and EP/X031624/1. T.G. acknowledges support from AWE via the Oxford Centre for High Energy Density Science (OxCHEDS). T.C. and S.M.V. acknowledge support from the Royal Society. A.F. acknowledges support from the STFC UK Hub for the Physical Sciences on XFELs. We thank the microscopy, x-ray diffraction and PVD platforms at IMPMC for support in producing and characterizing the $Fe_2O_3$ samples. We also thank T. De Resseguier, R. Smith, T. Vinci and A. Benuzzi-Mounaix for helpful discussions. This material is based upon work supported by the Department of Energy [National Nuclear Security Administration] University of Rochester "National Inertial Confinement Fusion Program" under Award Number(s) DE-NA0004144.

* AmourettiA@eie.eng.osaka-u.ac.jp
† celine.crepisson@physics.ox.ac.uk

[1] E. Bykova, L. Dubrovinsky, N. Dubrovinskaia, M. Bykov,

C. McCammon, S. V. Ovsyannikov, H. P. Liermann, I. Kupenko, A. I. Chumakov, R. Rüffer, M. Hanfland, and V. Prakapenka, Structural complexity of simple $Fe_2O_3$ at high pressures and temperatures, Nature Communications **7**, 10661 (2016).

[2] S. Ono and Y. Ohishi, In situ X-ray observation of phase transformation in $Fe_2O_3$ at high pressures and high temperatures, Journal of Physics and Chemistry of Solids **66**, 1714 (2005).

[3] S. Ono, T. Kikegawa, and Y. Ohishi, High-pressure phase transition of hematite, $Fe_2O_3$, Journal of Physics and Chemistry of Solids **65**, 1527 (2004).

[4] M. P. Pasternak, G. K. Rozenberg, G. Y. Machavariani, O. Naaman, R. D. Taylor, and R. Jeanloz, Breakdown of the Mott-Hubbard State in $Fe_2O_3$ : A First-Order Insulator-Metal Transition with Collapse of Magnetism at 50 GPa, Physical Review Letters **82**, 4663 (1999).

[5] J. Badro, G. Fiquet, V. V. Struzhkin, M. Somayazulu, H.-k. Mao, G. Shen, and T. Le Bihan, Nature of the High-Pressure Transition in $Fe_2O_3$ Hematite, Physical Review Letters **89**, 205504 (2002).

[6] A. Sanson, I. Kantor, V. Cerantola, T. Irifune, A. Carnera, and S. Pascarelli, Local structure and spin transition in $Fe_2O_3$ hematite at high pressure, Physical Review B **94**, 014112 (2016).

[7] E. Greenberg, I. Leonov, S. Layek, Z. Konopkova, M. P. Pasternak, L. Dubrovinsky, R. Jeanloz, I. A. Abrikosov, and G. K. Rozenberg, Pressure-Induced Site-Selective Mott Insulator-Metal Transition in $Fe_2O_3$, Physical Review X **8**, 031059 (2018).

[8] E. Bykova, M. Bykov, V. Prakapenka, Z. Konôpková, H.-P. Liermann, N. Dubrovinskaia, and L. Dubrovinsky, Novel high pressure monoclinic $Fe_2O_3$ polymorph revealed by single-crystal synchrotron X-ray diffraction studies, High Pressure Research **33**, 534 (2013).

[9] H. Liu, W. A. Caldwell, L. R. Benedetti, W. Panero, and R. Jeanloz, Static compression of alpha-$Fe_2O_3$: linear incompressibility of lattice parameters and high-pressure transformations, Physics and Chemistry of Minerals **30**, 582 (2003).

[10] P. Schouwink, L. Dubrovinsky, K. Glazyrin, M. Merlini, M. Hanfland, T. Pippinger, and R. Miletich, High-pressure structural behavior of $\alpha$-fe$_2$o$_3$ studied by single-crystal X-ray diffraction and synchrotron radiation up to 25 GPa, American Mineralogist **96**, 1781 (2011).

[11] G. K. Rozenberg, L. S. Dubrovinsky, M. P. Pasternak, O. Naaman, T. Le Bihan, and R. Ahuja, High-pressure structural studies of hematite $Fe_2O_3$, Physical Review B **65**, 064112 (2002).

[12] L. W. Finger and R. M. Hazen, Crystal structure and isothermal compression of $Fe_2O_3$, $Cr_2O_3$, and $V_2O_3$ to 50 kbars, Journal of Applied Physics **51**, 5362 (1980).

[13] E. Ito, H. Fukui, T. Katsura, D. Yamazaki, T. Yoshino, Y. Aizawa, A. Kubo, S. Yokoshi, K. Kawabe, S. Zhai, A. Shatzkiy, M. Okube, A. Nozawa, and K.-I. Funakoshi, Determination of high-pressure phase equilibria of $Fe_2O_3$ using the Kawai-type apparatus equipped with sintered diamond anvils, American Mineralogist **94**, 205 (2009).

[14] F. Coppari, R. F. Smith, J. Wang, M. Millot, D. Kim, J. R. Rygg, S. Hamel, J. H. Eggert, and T. S. Duffy, Implications of the iron oxide phase transition on the interiors of rocky exoplanets, Nature Geoscience **14**, 121 (2021).

[15] T. S. Duffy and R. F. Smith, Ultra-High Pressure Dynamic Compression of Geological Materials, Frontiers in Earth Science **7**, 23 (2019).

[16] T. Duffy, N. Madhusudhan, and K. Lee, Mineralogy of Super-Earth Planets, in *Treatise on Geophysics* (Elsevier, 2015) pp. 149–178.

[17] R. C. Liebermann and E. Schreiber, Elastic constants of polycrystalline hematite as a function of pressure to 3 kilobars, Journal of Geophysical Research **73**, 6585 (1968).

[18] K. Kondo, T. Mashimo, and A. Sawaoka, Electrical resistivity and phase transformation of hematite under shock compression, Journal of Geophysical Research **85**, 977 (1980).

[19] R. McQueen and S. Marsh, Handbook of Physical Constants (unpublished data), Geological Society of America Memoir **97**, 153 (1966).

[20] B. Nagler, B. Arnold, G. Bouchard, R. F. Boyce, R. M. Boyce, A. Callen, M. Campell, R. Curiel, E. Galtier, J. Garofoli, E. Granados, J. Hastings, G. Hays, P. Heimann, R. W. Lee, D. Milathianaki, L. Plummer, A. Schropp, A. Wallace, M. Welch, W. White, Z. Xing, J. Yin, J. Young, U. Zastrau, and H. J. Lee, The Matter in Extreme Conditions instrument at the Linac Coherent Light Source, Journal of Synchrotron Radiation **22**, 520 (2015).

[21] J. M. J. Madey, Stimulated Emission of Bremsstrahlung in a Periodic Magnetic Field, Journal of Applied Physics **42**, 1906 (1971).

[22] D. A. G. Deacon, L. R. Elias, J. M. J. Madey, G. J. Ramian, H. A. Schwettman, and T. I. Smith, First Operation of a Free-Electron Laser, Physical Review Letters **38**, 892 (1977).

[23] C. Prescher and V. B. Prakapenka, DIOPTAS : a program for reduction of two-dimensional X-ray diffraction data and data exploration, High Pressure Research **35**, 223 (2015).

[24] J. Kieffer, V. Valls, N. Blanc, and C. Hennig, New tools for calibrating diffraction setups, Journal of Synchrotron Radiation **27**, 558 (2020).

[25] L. M. Barker and R. E. Hollenbach, Laser interferometer for measuring high velocities of any reflecting surface, Journal of Applied Physics **43**, 4669 (1972).

[26] See Supplemental Material at [URL will be inserted by publisher] for more details on the experimental setup, characterization of the initial sample, VISAR analysis, and high-pressure phase identification. Further details on Birch-Murnaghan fit and the DFT+U calculations are also given. The Supplemental Material also contains Refs. [58–77], .

[27] R. Blake, R. Hessevick, T. Zoltai, and L. Finger, Refinement of the Hematite Structure, American Mineralogist **51**, 123 (1966).

[28] K. Ichiyanagi, S. Takagi, N. Kawai, R. Fukaya, S. Nozawa, K. G. Nakamura, K.-D. Liss, M. Kimura, and S.-i. Adachi, Microstructural deformation process of shock-compressed polycrystalline aluminum, Scientific Reports **9**, 7604 (2019).

[29] R. Briggs, M. Gorman, A. Coleman, R. McWilliams, E. McBride, D. McGonegle, J. Wark, L. Peacock, S. Rothman, S. Macleod, C. Bolme, A. Gleason, G. Collins, J. Eggert, D. Fratanduono, R. Smith, E. Galtier, E. Granados, H. Lee, B. Nagler, I. Nam, Z. Xing, and M. McMahon, Ultrafast X-Ray Diffraction Studies of the Phase Transitions and Equation of State

of Scandium Shock Compressed to 82 GPa, Physical Review Letters **118**, 025501 (2017).
[30] J. Barnes and S. Lyon, SESAME: the Los Alamos National Laboratory equation of state database, Los Alamos National Laboratory (1987).
[31] Y. B. Zel'dovich and Y. P. Raizer, Shock waves in solids, in *Physics of Shock Waves and High-Temperature Hydrodynamic Phenomena* (Elsevier, 1967) pp. 685–784.
[32] R. Mcqueen, S. Marsh, J. Taylor, J. Fritz, and W. Carter, The equation of state of solids from shock wave studies, in *High-Velocity Impact Phenomena* (Elsevier, 1970) pp. 293–417.
[33] M. G. Gorman, A. L. Coleman, R. Briggs, R. S. McWilliams, D. McGonegle, C. A. Bolme, A. E. Gleason, E. Galtier, H. J. Lee, E. Granados, M. Śliwa, C. Sanloup, S. Rothman, D. E. Fratanduono, R. F. Smith, G. W. Collins, J. H. Eggert, J. S. Wark, and M. I. McMahon, Femtosecond diffraction studies of solid and liquid phase changes in shock-compressed bismuth, Scientific Reports **8**, 16927 (2018).
[34] C. M. Pépin, A. Sollier, A. Marizy, F. Occelli, M. Sander, R. Torchio, and P. Loubeyre, Kinetics and structural changes in dynamically compressed bismuth, Physical Review B **100**, 060101 (2019).
[35] E. E. McBride, A. Krygier, A. Ehnes, E. Galtier, M. Harmand, Z. Konôpková, H. J. Lee, H.-P. Liermann, B. Nagler, A. Pelka, M. Rödel, A. Schropp, R. F. Smith, C. Spindloe, D. Swift, F. Tavella, S. Toleikis, T. Tschentscher, J. S. Wark, and A. Higginbotham, Phase transition lowering in dynamically compressed silicon, Nature Physics **15**, 89 (2019).
[36] R. F. Smith, J. H. Eggert, D. C. Swift, J. Wang, T. S. Duffy, D. G. Braun, R. E. Rudd, D. B. Reisman, J.-P. Davis, M. D. Knudson, and G. W. Collins, Time-dependence of the alpha to epsilon phase transformation in iron, Journal of Applied Physics **114**, 223507 (2013).
[37] R. F. Smith, J. H. Eggert, R. E. Rudd, D. C. Swift, C. A. Bolme, and G. W. Collins, High strain-rate plastic flow in Al and Fe, Journal of Applied Physics **110**, 123515 (2011).
[38] P. A. Cox, *Transition metal oxides: an introduction to their electronic structure and properties*, The International series of monographs on chemistry No. 27 (Clarendon Press ; Oxford University Press, Oxford : New York, 2010).
[39] C. S. Yoo, B. Maddox, J.-H. P. Klepeis, V. Iota, W. Evans, A. McMahan, M. Y. Hu, P. Chow, M. Somayazulu, D. Häusermann, R. T. Scalettar, and W. E. Pickett, First-Order Isostructural Mott Transition in Highly Compressed MnO, Physical Review Letters **94**, 115502 (2005).
[40] K. Ohta, R. E. Cohen, K. Hirose, K. Haule, K. Shimizu, and Y. Ohishi, Experimental and Theoretical Evidence for Pressure-Induced Metallization in FeO with Rocksalt-Type Structure, Physical Review Letters **108**, 026403 (2012).
[41] P. Hohenberg and W. Kohn, Inhomogeneous electron gas, Phys. Rev. **136**, B864 (1964).
[42] W. Kohn and L. J. Sham, Self-consistent equations including exchange and correlation effects, Phys. Rev. **140**, A1133 (1965).
[43] V. Anisimov, J. Zaanen, and O. Andersen, Band theory and mott insulators: Hubbard u instead of stoner i, Phys. Rev. B. **44**, 943 (1991).
[44] A. Liechtenstein, V. Anisimov, and J. Zaanen, Density-functional theory and strong interactions: Orbital ordering in mott-hubbard insulators, Phys. Rev. B **52**, R5467 (1995).
[45] S. Dudarev, G. Botton, S. Savrasov, C. Humphreys, and A. Sutton, Electron-energy-loss spectra and the structural stability of nickel oxide: An lsda+u study, Phys.Rev. B **57**, 1505 (1998).
[46] M. Cococcioni and S. de Gironcoli, Linear response approach to the calculation of the effective interaction parameters in the lda+u method, Phys. Rev. B **71**, 035105 (2005).
[47] J. Kuneš, D. M. Korotin, M. A. Korotin, V. I. Anisimov, and P. Werner, Pressure-Driven Metal-Insulator Transition in Hematite from Dynamical Mean-Field Theory, Physical Review Letters **102**, 146402 (2009).
[48] R. J. Husband, C. Strohm, K. Appel, O. B. Ball, R. Briggs, J. Buchen, V. Cerantola, S. Chariton, A. L. Coleman, H. Cynn, D. Dattelbaum, A. Dwivedi, J. H. Eggert, L. Ehm, W. J. Evans, K. Glazyrin, A. F. Goncharov, H. Graafsma, A. Howard, L. Huston, T. M. Hutchinson, H. Hwang, S. Jacob, J. Kaa, J. Kim, M. Kim, E. Koemets, Z. Konôpková, F. Langenhorst, T. Laurus, X. Li, J. Mainberger, H. Marquardt, E. E. McBride, C. McGuire, J. D. McHardy, M. I. McMahon, R. S. McWilliams, A. S. J. Méndez, A. Mondal, G. Morard, E. F. O'Bannon, C. Otzen, C. M. Pépin, V. B. Prakapenka, C. Prescher, T. R. Preston, R. Redmer, M. Roeper, C. Sanchez-Valle, D. Smith, R. F. Smith, D. Sneed, S. Speziale, T. Spitzbart, S. Stern, B. T. Sturtevant, J. Sztuk-Dambietz, P. Talkovski, N. Velisavljevic, C. Vennari, Z. Wu, C.-S. Yoo, U. Zastrau, Z. Jenei, and H.-P. Liermann, A MHz X-ray diffraction set-up for dynamic compression experiments in the diamond anvil cell, Journal of Synchrotron Radiation **30**, 671 (2023).
[49] G. Burns and A. Glazer, Space Group Applications, in *Space Groups for Solid State Scientists* (Elsevier, 2013) pp. 187–274.
[50] J. Badro, Spin Transitions in Mantle Minerals, Annual Review of Earth and Planetary Sciences **42**, 231 (2014).
[51] J.-F. Lin, S. Speziale, Z. Mao, and H. Marquardt, Effects of the electronic spin transitions of iron in lower mantle minerals: implications for deep mantle geophysics and geochemistry: spin transition in lower mantle., Reviews of Geophysics **51**, 244 (2013).
[52] B. Gan, G. Jiang, Y. Huang, H. Zhang, Q. Hu, and Y. Zhang, Phase diagram and thermoelastic property of iron oxyhydroxide across the spin crossover under extreme conditions, Physical Review B **107**, 064106 (2023).
[53] A. Amouretti, M. Harmand, B. Albertazzi, A. Boury, A. Benuzzi-Mounaix, D. A. Chin, F. Guyot, M. Koenig, T. Vinci, and G. Fiquet, Laser-driven shock compression and equation of state of Fe$_2$O$_3$ up to 700 GPa (2024), arXiv:2405.08350 [hep-ex].
[54] N. B. Zhang, Y. Cai, X. H. Yao, X. M. Zhou, Y. Y. Li, C. J. Song, X. Y. Qin, and S. N. Luo, Spin transition of ferropericlase under shock compression, AIP Advances **8**, 075028 (2018).
[55] S. Pandolfi, S. B. Brown, P. G. Stubley, A. Higginbotham, C. A. Bolme, H. J. Lee, B. Nagler, E. Galtier, R. L. Sandberg, W. Yang, W. L. Mao, J. S. Wark, and A. E. Gleason, Atomistic deformation mechanism of silicon under laser-driven shock compression, Nature Communications **13**, 5535 (2022).

[56] M. O. Schoelmerich, T. Tschentscher, S. Bhat, C. A. Bolme, E. Cunningham, R. Farla, E. Galtier, A. E. Gleason, M. Harmand, Y. Inubushi, K. Katagiri, K. Miyanishi, B. Nagler, N. Ozaki, T. R. Preston, R. Redmer, R. F. Smith, T. Tobase, T. Togashi, S. J. Tracy, Y. Umeda, L. Wollenweber, T. Yabuuchi, U. Zastrau, and K. Appel, Evidence of shock-compressed stishovite above 300 GPa, Scientific Reports **10**, 10197 (2020).

[57] J. Hernandez, G. Morard, M. Guarguaglini, R. Alonso-Mori, A. Benuzzi-Mounaix, R. Bolis, G. Fiquet, E. Galtier, A. E. Gleason, S. Glenzer, F. Guyot, B. Ko, H. J. Lee, W. L. Mao, B. Nagler, N. Ozaki, A. K. Schuster, S. H. Shim, T. Vinci, and A. Ravasio, Direct Observation of Shock-Induced Disordering of Enstatite Below the Melting Temperature, Geophysical Research Letters **47**, 10.1029/2020GL088887 (2020).

[58] A. Descamps, B. K. Ofori-Okai, O. Bistoni, Z. Chen, E. Cunningham, L. B. Fletcher, N. J. Hartley, J. B. Hastings, D. Khaghani, M. Mo, B. Nagler, V. Recoules, R. Redmer, M. Schörner, D. G. Senesky, P. Sun, H.-E. Tsai, T. G. White, S. H. Glenzer, and E. E. McBride, Evidence for phonon hardening in laser-excited gold using x-ray diffraction at a hard x-ray free electron laser, Science Advances **10**, eadh5272 (2024).

[59] L. Lutterotti, Maud (material analysis using diffraction) version 2.33, https://luttero.github.io/maud, (2010).

[60] W. A. Dollase, Correction of intensities for preferred orientation in powder diffractometry: application of the March model, Journal of Applied Crystallography **19**, 267 (1986).

[61] R. Ramis, R. Schmalz, and J. Meyer-Ter-Vehn, Multi— a computer code for one-dimensional multigroup radiation hydrodynamics, Computer Physics Communications **49**, 475 (1988).

[62] X. Cao, Y. Wang, X. Li, L. Xu, L. Liu, Y. Yu, R. Qin, W. Zhu, S. Tang, L. He, C. Meng, B. Zhang, and X. Peng, Refractive index and phase transformation of sapphire under shock pressures up to 210 GPa, Journal of Applied Physics **121**, 115903 (2017).

[63] S. H. Glenzer, L. B. Fletcher, E. Galtier, B. Nagler, R. Alonso-Mori, B. Barbrel, S. B. Brown, D. A. Chapman, Z. Chen, C. B. Curry, F. Fiuza, E. Gamboa, M. Gauthier, D. O. Gericke, A. Gleason, S. Goede, E. Granados, P. Heimann, J. Kim, D. Kraus, M. J. MacDonald, A. J. Mackinnon, R. Mishra, A. Ravasio, C. Roedel, P. Sperling, W. Schumaker, Y. Y. Tsui, J. Vorberger, U. Zastrau, A. Fry, W. E. White, J. B. Hasting, and H. J. Lee, Matter under extreme conditions experiments at the Linac Coherent Light Source, Journal of Physics B: Atomic, Molecular and Optical Physics **49**, 092001 (2016).

[64] A. Flacco and T. Vinci, https://github.com/neutrinotoolkit/neutrino, (2013).

[65] T. De Rességuier, P. Berterretche, and M. Hallouin, Influence of quartz anisotropy on shock propagation and spall damage, International Journal of Impact Engineering **31**, 545 (2005).

[66] C. Crépisson, A. Amouretti, M. Harmand, C. Sanloup, P. Heighway, S. Azadi, D. McGonegle, T. Campbell, J. Pintor, D. A. Chin, E. Smith, L. Hansen, A. Forte, T. Gawne, H. J. Lee, B. Nagler, Y. Shi, G. Fiquet, F. Guyot, M. Makita, A. Benuzzi-Mounaix, T. Vinci, K. Miyanishi, N. Ozaki, T. Pikuz, H. Nakamura, K. Sueda, T. Yabuuchi, M. Yabashi, J. S. Wark, D. N. Polsin, and S. M. Vinko, Shock-driven amorphization and melting in $Fe_2O_3$, Physical Review B **111**, 024209 (2025).

[67] L. S. Dubrovinsky, N. A. Dubrovinskaia, C. McCammon, G. K. Rozenberg, R. Ahuja, J. M. Osorio-Guillen, V. Dmitriev, H.-P. Weber, T. L. Bihan, and B. Johansson, The structure of the metallic high-pressure Fe $_3$ O $_4$ polymorph: experimental and theoretical study, Journal of Physics: Condensed Matter **15**, 7697 (2003).

[68] Q. Hu, D. Y. Kim, W. Yang, L. Yang, Y. Meng, L. Zhang, and H.-K. Mao, FeO2 and FeOOH under deep lower-mantle conditions and Earth's oxygen–hydrogen cycles, Nature **534**, 241 (2016).

[69] B. Lavina and Y. Meng, Unraveling the complexity of iron oxides at high pressure and temperature: Synthesis of Fe5O6, Science Advances **1**, e1400260 (2015).

[70] B. Lavina, P. Dera, E. Kim, Y. Meng, R. T. Downs, P. F. Weck, S. R. Sutton, and Y. Zhao, Discovery of the recoverable high-pressure iron oxide Fe4O5, Proceedings of the National Academy of Sciences **108**, 17281 (2011).

[71] P. Giannozzi and et al., Quantum espresso: a modular and open-source software project for quantum simulations of materials, Journal of physics: Condensed matter **39**, 395502 (2009).

[72] P. G. et al., Advanced capabilities for materials modelling with quantum espresso, J. Phys.: Condens. Matter **29**, 465901 (2017).

[73] A. D. Corso, Pseudopotentials periodic table: From h to pu, Computational Materials Science **95**, 337 (2014).

[74] J. P. Perdew, A. Ruzsinszky, G. I. Csonka, O. A. Vydrov, G. E. Scuseria, L. A. Constantin, X. Zhou, and K. Burke, Restoring the density-gradient expansion for exchange in solids and surfaces, Phys. Rev. Lett. **100**, 136406 (2008).

[75] D. Benjelloun, J.-P. Bonnet, J.-P. Doumerc, J.-C. Launay, M. Onillon, and P. Hagenmuller, Mater. Chem. Phys. **10**, 503 (1984).

[76] J. M. D. Coey and G. A. Sawatzky, J. Phys. C **4**, 2386 (1971).

[77] D. B. Ghosh and S. de Gironcoli, Structural and spin transitions in $Fe_2O_3$, arXiv:0903.2104 [cond-mat] (2009), arXiv: 0903.2104.